Adatoms, dimers, and interstitials on group-IV(113) surfaces: First-principles studies of energetical, structural, and electronic properties

A. A. Stekolnikov, J. Furthmüller, and F. Bechstedt
Institut für Festkörpertheorie und Theoretische Optik, Friedrich-Schiller-Universität, Max-Wien-Platz 1, 07743 Jena, Germany
(Received 20 December 2002; published 28 May 2003)

Using an *ab initio* plane-wave-pseudopotential code we study a variety of 3×1 and 3×2 reconstructions including adatom (A), dimer (D), and interstitial (I) models of Ge, Si, and diamond(113) surfaces. All reconstruction elements give rise to local minima on the total-energy surface. For Ge and Si, interstitial reconstructions are confirmed to be most favorable. Reconstructions without interstitials, even the oppositely puckered 3×2 AD model, do not open a surface-state gap. The semiconducting 3×2 ADI structure is the lowest one in energy for Si, since the occupied surface states appear below the valence-band maximum. The 3×2 AI surface with asymmetric pentamers is also semiconducting and, in the Ge case, it is even lower in energy. The 3×1 AD model is found to be the most stable (113) surface reconstruction for diamond, despite the vanishing gap. The measured structural data, the observed (in particular occupied) surface states, the scanning-tunneling microscopy images of Si and Ge(113)3×2 and 3×1 surfaces, as well as the temperature-induced phase transitions can widely be explained using models with subsurface interstitial atoms and accounting for the mobility of such atoms.

DOI: 10.1103/PhysRevB.67.195332 PACS number(s): 68.35.Bs, 68.35.Md, 73.20.At

I. INTRODUCTION

High-index (113) surfaces of group-IV semiconductors are of interest from both the fundamental and applied points of view. In recent years wide flat (113) terraces have been prepared on Si substrates demonstrating that such surfaces are thermally stable against faceting.[1] Their inherent structural anisotropy makes (113) surfaces promising substrates for epitaxial growth of optoelectronic devices.[2] Observations of (113) facets on Ge islands grown on Si(111), Si(100), or SiC(0001) substrates indicate the stability of (113) surfaces also for germanium.[3–5] The interest in diamond(113) surfaces is mainly fundamental. However, (113) facets have been observed on small diamond crystals grown by chemical vapor deposition techniques.[6]

The actual atomic structure of the (113) surfaces is strongly influenced by the surface reconstruction. For the weaker bonded group-IV materials, in particular, Si and Ge, 3×1 and 3×2 translational symmetries have been reported.[7–28] To our knowledge there is neither a theoretical nor an experimental study of clean reconstructed C(113) surfaces. The Si(113) surface exhibits a 3×2 reconstruction at room temperature, while a transition to the 3×1 phase is observed at elevated temperature.[10,13,15,23,24] In the Ge case 3×2 and 3×1 periodicities seem to coexist already at room temperature.[14,18,28]

The bulk-terminated (113) surfaces of diamond-structure crystals consist of alternating rows of twofold-coordinated (001)-like atoms and threefold-coordinated (111)-like atoms. If one (001)-like atom is removed, the adjacent (111)-like atom looks like an adatom (A). The additional formation of a dimer (D) by two (001)-like atoms leads to 3×1 translational symmetry.[7] Many refinements of such an adatom-dimer (AD) model, including voids, puckering, buckling, and vertical displacement of the dimers, have been discussed to explain the observed 3×2 translational symmetry, particularly for Si.[7,8,17,20–23,25] One important step towards understanding the behavior of group-IV(113) surfaces was the introduction of an additional reconstruction element, a sixfold-coordinated surface self-interstitial (I) similar to the [110]-split interstitial bulk defects, by Dabrowski *et al.*[11,26,27] Interstitial distribution and migration[14,27,28] allow the study of additional surface reconstructions, among them adatom-interstitial (AI) and adatom-dimer-interstitial (ADI) models.

Meanwhile, there are several *ab initio* studies of 3×1 and 3×2 reconstructions of Si and Ge(113) surfaces.[25–29,31] There are also studies using a semiempirical method[30] or combined methods.[25] The energetical ordering of the most important structural models is clarified for both Si and Ge.[11,25,28] However, the absolute values of the resulting surface energies have to be well converged. Their comparison with energies of low-index surfaces provides information on whether (113) facets appear on equilibrium crystal shapes and, hence, are really stable. The bonding energies of the interstitials may allow a discussion of the temperature-induced phase transitions. Details of the geometrical reconstructions concerning their asymmetries, e.g., buckling, puckering, vertical displacement of appearing reconstruction elements, tetramers, or pentamers, are under discussion. The chemical trends in energies and geometrical parameters are not understood. This holds for the comparison between Si and Ge(113) but, in particular, for C(113); the properties of this surface are unknown.

The driving forces of the various reconstructions concern unsolved problems. The relationship between energetics, bonding, displacements of atoms, and the electronic structure is not clarified. There are a few simulated images observable in scanning-tunneling microscopy (STM).[11,25–27] However, their relation to the surface band structures and surface electronic states is not derived. Calculated band structures are not published, except from those within a tight-binding approach,[25] the accuracy of which is, however, limited. The experimental bands for Si(113)3×2 need an

interpretation.[21] It has to be discussed why 3×1 reconstructions are seemingly observed in several experiments, despite the violation of the general reconstruction rules[32] and the electron counting rule.[33] Consequently, the metallic or insulating character of a (113) surface has to be explained depending on the translational symmetry but also on the (local) point-group symmetry.

In this contribution results of well-converged first-principles calculations are presented for the most important reconstruction models. The atomic structure, the energetics, and the electronic states are studied. The stability of the (113) surfaces is discussed in terms of absolute surface energies and their comparison with those of other orientations. The energetical ordering is related to the reconstruction elements, the geometry, and the resulting band structures. The driving forces of reconstructions and their chemical trends are derived. The resulting structural parameters, band structures, and STM images are discussed in light of available experimental data.

II. COMPUTATIONAL METHODS

A. Total-energy and electronic-structure calculations

The calculations are performed within the density-functional theory[34] (DFT) in the local-density approximation (LDA).[35] The electron-electron interaction is described by the Ceperley-Alder functional as parametrized by Perdew and Zunger.[36] In the case of diamond(113) surfaces several results are checked by repeating the calculations taking generalized gradient corrections within the generalized gradient approximation[37] into account. The interaction of the electrons with the atomic cores is treated by non-norm-conserving *ab initio* Vanderbilt pseudopotentials.[38] Nonlinear core corrections are also taken into account.[39] The non-norm-conserving pseudopotentials allow a substantial potential softening even for the first-row element carbon.[40] As a consequence the plane-wave expansion of the single-particle eigenfunctions is restricted to low kinetic-energy cutoffs 8.8 Ry (Ge), 9.6 Ry (Si), and 19.8 Ry (C).

In the explicit computations we use the Vienna *ab initio* simulation package (VASP).[41] In the bulk case the DFT-LDA yields cubic lattice constants of $a_0=5.627$, 5.398, and 3.531 Å and indirect fundamental energy gaps $E_g=0.00$, 0.46, and 4.15 eV for Ge, Si, and diamond, respectively.[42] Quasiparticle corrections[43,44] are not added to the Kohn-Sham eigenvalues[35] of the DFT-LDA in order to account for the excitation aspect. In this approximation and without considering the spin polarization of the free atoms, chemical potentials μ of the constituents (i.e., negative cohesive energies) follow to be $\mu=-5.195$, -5.957, and -10.947 eV/atom, respectively, for Ge, Si, and C.

The surfaces are modeled by repeated slabs. Each slab consists of 11 double layers and the same amount of vacuum layers. Always a 3×2 lateral unit cell is used, even studying the nominal 3×1 translational symmetry. The bottom sides of the slabs are passivated by hydrogen atoms and kept frozen during the surface optimization. The topmost six double layers of the slab are allowed to relax. Four (eight) **k** points are used in the irreducible part, i.e., in a quarter (one-half) of the Brillouin zone (BZ) for the surfaces with 3×2 translational symmetry. In order to derive well-converged absolute surface energies, larger centrosymmetric supercells with 42 bilayers and 46 vacuum layers are also studied. This approach has been tested to give converged energies for other surface orientations of group-IV semiconductors.[42] In particular, the weakly bonded Ge requires many layers to achieve convergence.

The eigenvalues and eigenfunctions of the Kohn-Sham equation[35] are used to calculate the local electronic density of states and the STM images within the Tersoff-Hamann approach.[45] A constant-height mode is assumed for the simulation. Smearing-out procedures to account for the nonideality of the tip are not used. Also no energetical shift towards higher (lower) energies of the empty (occupied) states is applied in order to account for the quasiparticle character of the involved electronic states.[43,44]

B. Reconstruction models and structural parameters

A (113) surface of a truncated bulk crystal of a Ge, Si, or diamond crystal consists of alternating (001)- and (111)-like atomic rows in the uppermost double layer [Fig. 1(a)]. A 1×1 unit cell contains two atoms. The (001)-like atoms in the upper part of this bilayer are twofold coordinated and, hence, possess two dangling bonds (DBs). The (111)-like atoms in the slightly lower part of the topmost bilayer are threefold coordinated and, therefore, only have one DB. The DBs are half filled. According to the general rules[32] such a surface should reconstruct to minimize the DB density and the surface energy.

The removal of every third (001)-like atom in the $[1\bar{1}0]$ direction gives a 3×1 translational symmetry. The adjacent (111)-like atom rebonds and forms an adatomlike reconstruction element. The adatom is characterized by the displacements Δz_{ad} and Δy_{ad} parallel to the [113] or $[33\bar{2}]$ direction from the bulklike position. The two twofold-coordinated atoms remaining in a 3×1 cell form a dimer along the $[1\bar{1}0]$ direction with a characteristic bond length d_{dim} and a possible dimer tilting Δz_{dim} [Fig. 1(b)]. The two (σ and π) bonding orbitals of the dimer are fully occupied with electrons. Together with the two adjacent nonrebonded edge atoms they form a trapezoidal tetramer. A possible asymmetry may be characterized by the difference Δz_{edge} of the vertical positions of the two edge atoms. It results in an AD reconstruction model, keeping the 3×1 translational symmetry [Fig. 1(b)].[7]

Refinements of the AD model such as dimer tilting or puckering (indicated by Δz_{dim} and $\Delta z_{\mathrm{edge}}\neq0$) may lower the total energy, but still the electron counting rule[32,33] cannot be fulfilled. Three partially filled DBs remain. However, if the dimers [as in the case of Ge and Si(001)$c(4\times2)$ or $p(2\times2)$ surfaces] of adjacent horizontal rows are tilted/puckered (p) in opposite directions,[7,25] it results in a 3×2 periodicity that allows for pairing of all electrons and, hence, an insulating (semiconducting) surface.[25] The generalized oppositely puckered 3×2 AD(op) structure is shown in Fig. 1(c).

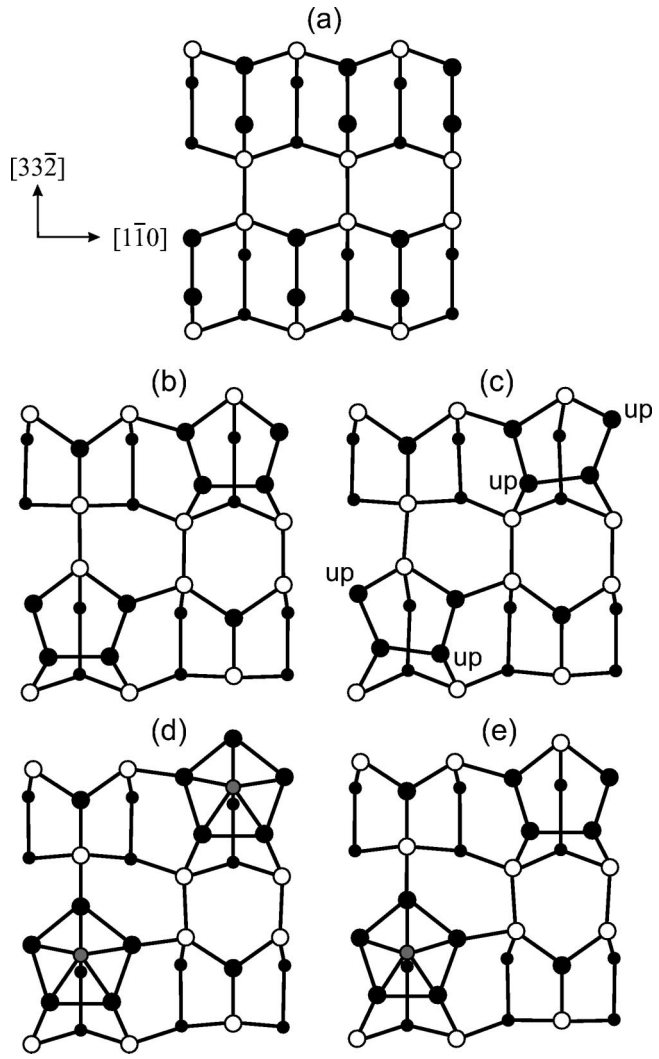

FIG. 1. Top view of various reconstructions of (113) surfaces. The area of a 3×2 unit cell is shown. (a) Bulk-truncated surface with possible relaxations, (b) 3×1 AD model, (c) 3×2 AD [oppositely puckered (op)] structure, (d) 3×1 or 3×2 AI reconstruction, and (e) 3×2 ADI model. Filled (open) circles indicate atoms in the top (second) bilayer. Dots represent atoms in the third bilayer. The interstitial atoms are indicated by shaded circles.

The 3×1 AD surface can transform into another metastable structure by capturing a self-interstitial atom in the center of the tetramer. It results in a 3×1 AI reconstruction [Fig. 1(d)].[26] The interstitial atom is sixfold coordinated. Together with the (subsurface) common neighbor (called the subatom) of the two edge atoms, the original tetramer forms a nearly flat pentamer around the interstitial. The subatom is characterized by the vertical distance to the average position of the edge atoms Δz_{sub}. The interstitial may be characterized by the vertical distance Δz_{in} of this atom to the average position of the atoms in the surrounding pentamer. A possible displacement along the $[1\bar{1}0]$ direction is represented by Δx_{in}. However, there is also substantial interaction with the atom beneath in the third bilayer, completing the sixfold coordination. The number of DBs is not reduced with respect to the 3×1 AD surface. Complete electron pairing or completely empty orbitals may occur by allowing an asymmetry associated, e.g., with the opposite tilting of neighboring pentamers, or with different vertical positions of atoms in adjacent pentamers. The resulting 3×2 AI reconstruction [also Fig. 1(d)] should be insulating. For that reason, we study asymmetric 3×2 AI reconstructions. The AD and AI models differ by the weakly bonded interstitial atoms. The migration of such atoms is likely, resulting in a certain surface disorder. A stable intermediate structure may only contain one interstitial per 3×2 cell. It results in the mixed 3×2 ADI reconstruction shown in Fig. 1(e).[26] Since there is an even number of half-filled DBs, also this combined reconstruction model may describe a nonmetallic surface.

III. RESULTS AND DISCUSSION

A. Energetics and geometries

The calculated surface energies are summarized in Table I. Important geometry parameters are listed in Table II. In addition to the most stable reconstruction models AD, ADI, and AI, which represent 3×1 and 3×2 translational symmetries with different symmetric and asymmetric variations, we have also studied the bulk-terminated and relaxed (113) surfaces. The relaxation of the bulk-terminated surfaces gives rise to a significant reduction of the absolute surface energies. Dimerization of two twofold-coordinated atoms

TABLE I. Absolute surface energies of Ge, Si, and diamond(113)3×1 and 3×2 surfaces per 3×2 unit cell (E_{surf}) or per unit area (γ). (p): puckered, (op): oppositely puckered.

Reconstruction	E_{surf} (eV/3×2 cell)			γ (J/m^2)		
	C	Si	Ge	C	Si	Ge
Bulk terminated	32.28	20.00	15.83	8.34	2.21	1.61
Relaxed	26.44	16.71	12.70	6.83	1.85	1.29
3×1 AD	21.29	13.49	10.58	5.50	1.49	1.08
3×1 AD(p)		13.37	10.44		1.48	1.06
3×2 AD(op)		13.35	10.42		1.48	1.06
3×1 AI		13.16	9.77		1.45	0.99
3×2 AI		13.11	9.72		1.45	0.99
3×2 ADI		12.69	9.77		1.40	0.99

TABLE II. Important geometry parameters of 3×1 and 3×2 reconstructions of (113) surfaces of Si and Ge (in units of the bulk bond length). Due to the asymmetry in the cases of 3×2 AI and ADI, two values are given for the left(right) part of the reconstructed unit cell [Figs. 2(d) and 2(e)]. For the 3×2 AD(op) only one value of each tilting parameter Δz_{dim} and Δz_{edge} is given, since the buckling in the opposite tetramer only gives a changed sign. In the 3×1 AD case diamond parameters are given for comparison.

Reconstruction	Element	Dimer atoms		Edge atom	Subatom	Adatom		Interstitial	
		d_{dim}	Δz_{dim}	Δz_{edge}	Δz_{ad}	Δz_{sub}	Δy_{ad}	Δz_{in}	Δx_{in}
3×1 AD	C	0.96	0	0	−0.22	−0.19	−0.29		
	Si	1.00	0	0	−0.21	−0.19	−0.36		
	Ge	1.06	0	0	−0.22	−0.01	−0.34		
3×2 AD(op)	Si	0.99	0.23	0.26	−0.34	−0.19	−0.37		
	Ge	1.01	0.29	0.27	0.00	−0.34	−0.37		
3×1 AI	Si	0.98	0	0	0.00	0.00	−0.28	0.62	0
	Ge	1.00	0	0	0.09	0.04	−0.28	0.63	0
3×2 AI	Si	0.99(0.99)	0.02(0.05)	0.06(0.21)	0.03(0.00)	0.00(−0.01)	−0.27(−0.25)	0.61(0.60)	−0.03(0.10)
	Ge	1.00(1.02)	0.0(0.09)	0.01(0.26)	0.09(0.01)	0.02(0.04)	−0.26(0.27)	0.61(0.63)	−0.01(0.12)
3×2 ADI	Si	1.01(0.98)	0	0	0.03(−0.19)	−0.01(−0.02)	−0.28(−0.34)	0.62	0
	Ge	1.00(1.06)	0	0	0.08(−0.21)	0.04(0.01)	−0.29(−0.33)	0.64	0

and the removal of each third one reduce the number of dangling bonds and stabilize the surface structure. Consequently, the 3×1 AD model lowers the surface energy substantially independent of the group-IV material considered. The dimerization gains energy, as in the case of $(001)2\times1$ surfaces as follows by comparison of the surface energies for the relaxed and 3×1 AD geometries. Despite the contribution of the adatom, the energy gains per dimer of about 2.6 (C), 1.6 (Si), and 1.1 eV (Ge) are somewhat smaller than the corresponding values for the $(001)2\times1$ surfaces.[42] In the case of Ge but also for Si, this should be partly a consequence of the larger dimer bond lengths on (113) surfaces with $d_{\mathrm{dim}}=1.00$ or 1.06 d_{bulk} (see Table II) for Si or Ge.

Further refinements of the 3×1 AD reconstruction do not reduce the surface energy or do not give rise to another local minimum on the total-energy surface in the case of diamond. Asymmetries in the reconstruction such as buckling or puckering are not energetically favorable because of the strain induced in the subsurface region. These observations are similar to those made previously for diamond $(111)2\times1$ and $(001)2\times1$ surfaces.[42,46,47] Interstitial atoms are not bonded on a diamond(113) surface. They are energetically unfavorable as the adatoms in the case of the C(111) surface.[42,48] As a consequence, among the reconstruction models considered in Table I the 3×1 AD structure is the only stable geometry for diamond, despite the violation of the electron counting rule.

The crystals of the other group-IV elements, Si and Ge, have much softer bonds than diamond. Asymmetric reconstructions are likely as in the case of the low-index surfaces.[42,46] Asymmetric atomic displacements parallel to the surface normal give rise to surface buckling. Indeed, such displacements lower the surface energy. For Si and Ge, puckered 3×1 and 3×2 AD models introduce additional structural degrees of freedom. In the 3×1 structure, diagonal atoms in the tetramer are buckled towards the same direction. In the oppositely puckered 3×2 AD geometry upper and lower atoms of two tetramers belong to different diagonals. The resulting buckling amplitudes of the dimer atoms but also of the edge atoms (cf. Table II) are of the same order of magnitude as observed for the dimers on (001) surfaces and the chains on (111) surfaces.[42,46] Apart from signs, the geometry parameters are almost the same for 3×1 AD(p) and 3×2 AD(op) models. Only in the Ge case is one parameter somewhat different for 3×1 and 3×2 unit cells, and that is the buckling Δz_{edge} between the edge atoms (instead of 0.27, it is 0.17 d_{bulk}). Indeed, puckering reduces the surface energy. For silicon we calculate an energy gain of 0.12 eV per 3×2 unit cell for the 3×1 AD(p) reconstruction. The puckered structure with 3×1 translational symmetry is only slightly higher in energy by 0.02 eV compared with the 3×2 AD(op) reconstruction. Similar energy gains are obtained for germanium (cf. Table I). The 3×1 puckered model lowers the surface energy by 0.14 eV for Ge. Opposite puckering further lowers the surface energy by 0.02 eV, a value of the order of the thermal energy at room temperature. Consequently, a flipping of the tetramers should be already possible at room temperature. A phase transition between 3×1 and 3×2 structures may be easily imaginable in the framework of the AD model as suggested in the literature for Si.[20,25] The small energy differences also suggest the local coexistence of phases with different translational symmetries, as observed in the Ge case.[14,18,28]

The introduction of self-interstitials on Si and Ge(113) surfaces reduces the energy further, in agreement with previous calculations.[26,28] However, there is a sensitive balance of different energy contributions. For Si(113), the 3×2 ADI reconstruction [Fig. 1(e)] with only one interstitial atom per 3×2 unit cell gives the lowest-energy structure. The 3×1 and 3×2 AI structures with more interstitials per unit area are less stable. With respect to the optimized 3×2 AD(op) structure (Table I), the adsorption of an interstitial atom gains energy of about 0.7 eV within the 3×2 ADI model. Due to the repulsive interaction of the interstitials on the short distances this value is reduced to 0.2 eV per interstitial for AI geometries. For Ge the energies of the 3×1 AI and 3×1

ADI models are equal. The novel asymmetric 3×2 AI model gives rise to the lowest-energy structure. There is an energetical ordering 3×1 AI/3×2 ADI and 3×2 AI, which is different from that observed for Si(113). The repulsive interaction of the interstitials is much weaker in the germanium case. The energy gain of 0.6 eV by adding an Ge interstitial in a 3×2 ADI structure is reduced to 0.3 eV per interstitial in the AI cases.

Within the interstitial models pronounced asymmetries are found, but only for the 3×2 AI reconstruction (cf. Table II). There is a general tendency to break the symmetry between the two pentamers. Such asymmetries have been observed in STM images for the seemingly 3×1 reconstruction.[28] The unit cell of the 3×2 AI reconstruction is doubled by opposite buckling of the two pentamers, where the interstitial atoms can also change their central positions. Such a staggered arrangement of buckled pentamers lowers the total energy by about 50 meV for Si and Ge and results in the 3×2 AI model. Here we present the most favorable asymmetries found. Other asymmetries, e.g., an average relative vertical displacement of the two pentamers within the 3×2 AI model, also lower the total energy. One observes different local minima on the total-energy surface with practically the same surface energies. The band structures of the two geometries are nearly identical. Particularly for Si the asymmetry opens a gap. The removal of one interstitial, i.e., the transition to the 3×2 ADI structure, further lowers the energy in the Si case but not for Ge(113). For the 3×2 ADI reconstruction an additional asymmetry is not favorable for both materials.

The small energetical differences between ADI and AI models may explain the observed temperature-induced order-disorder phase transitions.[10,13–15,18,23,24,28] The low temperature of about 120 K for Ge and the high temperature of about 800 K for Si seem to be correlated with the differences in the corresponding surface energies between AI and ADI structures. According to the small binding energy of the second interstitial, surface diffusion must play an important role, in particular the migration of the interstitial atoms.[28] Such a migration at a certain temperature may be accompanied by a certain amount of surface disorder and, hence, explains the coexistence of 3×1 and 3×2 reconstructed domains on a given (113) surface.[13,16,18,20,28] In the Si(113) case the observation of 3×1 instead of 3×2 seems to be also dependent on the density of the surface defects and the bulk doping.[8,12]

The energetical ordering of the reconstruction models in Table I is the same as in other *ab initio* calculations,[11,25,26,28] apart from the fact that the asymmetric 3×2 AI structure has not been clarified. In particular, interstitial models give the lowest-energy structures. We agree that 3×2 ADI is the lowest-energy structure for Si(113) and with nearly the same energies for all interstitial reconstructions of Ge(113). However, the calculated absolute surface energies per unit area, γ, in Table I are slightly smaller than those computed by other authors.[11,26,28] This holds for both Si and Ge(113). This is mostly related to the large number of atomic layers needed to obtain convergence, in particular, for Ge,[42] and the difficulties in determining the absolute energies.

Because of the high accuracy of our calculations the absolute surface energies can be compared with those obtained for other surface orientations and used in a Wulff construction of the equilibrium crystal shape (ECS).[49,50] For diamond the absolute surface energy of 5.50 J/m^2 lies between 4.06 J/m^2 for $(111)2\times1$ and 5.71 J/m^2 for $(001)2\times1$.[42] Consequently, the ECS shows small (113) areas, indicating the stability of this facet also for diamond crystals.[6] For Si, (113) and (001) surfaces possess nearly the same energy, 1.40 and 1.41 J/m^2. The experimental values, $\gamma_{113}=1.38$ J/m^2 and $\gamma_{001}=1.36$ J/m^2,[1] are also very similar and agree with respect to the vanishing energy variation between the two orientations. For the (111) cleavage face[42] the surface energy $\gamma_{111}=1.36$ J/m^2 is of course lower. Facets with all these surface orientations [including (110), in addition] occur on the ECS, indicating the stability of the Si(113) surface against faceting into low-index surfaces.[50] In the Ge case we find the lowest surface energy of 0.99 J/m^2 for the (113) orientation. However, the energies 1.01 and 1.00 J/m^2 for (111) and (100), respectively, are nearly the same within the accuracy of the calculations. Consequently, there is a tendency for a more or less spherical ECS. In the thermodynamic equilibrium Ge nanocrystals with (113) facets should be also observable, indicating their stability. We have to note that for both Si and Ge further reduction of energies of (113) surfaces is not expected, because of the similarity with the energies of the (111) cleavage faces.

B. Band structures and electronic states

In order to understand the driving forces of the reconstructions and the electronic structures of the (113) surfaces for Si and Ge, we plot the band structures obtained within DFT-LDA in Fig. 2 for all important models. In principle, a similar behavior is observed for Si and Ge. Modifications are related to differences in the bulk band structures. For Ge a small direct gap at Γ and a conduction-band minimum at L instead of at 0.85 ΓX are found. The minima at L points are responsible for the deep projected conduction bands at the K point of the surface BZ. Moreover, the weaker bonding in Ge plays a role. The 3×1 AD model [Fig. 2(a)] clearly indicates metallic behavior of the (113) surfaces, in agreement with the three half-filled (without buckling) DBs. DB-related bands overlap partially with bulk states near the valence-band maximum (VBM). The Fermi level at an energy near the VBM crosses these bands. A similar behavior is observed for the lowest-energy AD structure of the C(113)3×1 surface. The metallic character remains true for the puckered AD, but surprisingly also for the oppositely puckered 3×2 AD structures [Fig. 2(b)]. The DBs at the adatoms still weakly interact and the splitting of the two bands due to asymmetric displacements and DB interaction is too small. This is in contrast to the band structure obtained within a tight-binding approximation by Wang *et al.*[25] A surface-state gap of about 1 eV (Ref. 25) would require remarkable differences in the *s* and *p* character of the two DBs at the adatoms. Still partially occupied states belong to adatoms, and there is not a significant tendency to transfer electrons from tetramers to the adatoms.

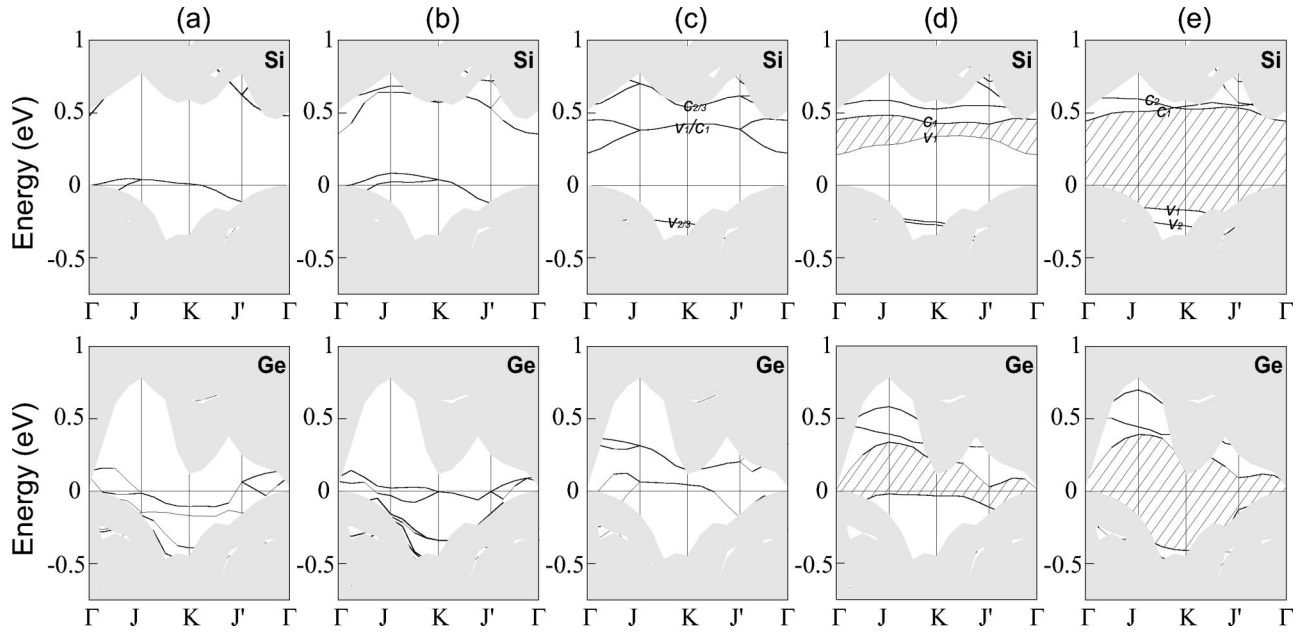

FIG. 2. Band structures of Si and Ge(113) surfaces. The shaded regions indicate the projected bulk band structures. Surface bound-state bands are shown as solid lines. Fundamental gaps between such states are represented as hatched regions. (a) 3×1 AD, (b) 3×2 AD(op), (c) 3×1 AI, (d) 3×2 AI, and (e) 3×2 ADI. In all cases the BZ of the 3×2 reconstruction is used for the presentation. For Si(113) in (c)–(e), surface bands are denoted by v_i and c_i.

Adding a surface self-interstitial but keeping the 3×1 translational symmetry in the 3×1 AI structure no change in metallicity occurs. In the upper part of the fundamental gap in the projected bulk band structure appears a half-filled band pair that is degenerate along the BZ boundaries and pins the Fermi level [Fig. 2(c)]. However, giving the system more degrees of freedom in a 3×2 AI structure and allowing an asymmetric behavior of the two pentamers in the 3×2 unit cell (relative vertical displacement and/or opposite buckling) results in the degeneracy being lifted and the appearance of a surface-state gap [Fig. 2(d)]. The fully occupied band moves down in energy. Therefore, the stabilization of the 3×2 translation symmetry with respect to the 3×1 one, in Table I, can be explained by an accompanying gain of band-structure energy. The removal of one interstitial atom within the 3×2 ADI reconstruction model increases the asymmetries in the 3×2 unit cells. The insulating or semiconducting character of the surface is increased by further opening the surface-state gap for both Si and Ge(113) [Fig. 2(e)]. The highest occupied surface-state band completely moves below the VBM. There is only a measurable total-energy gain for Si (cf. Table I), which is related to the lowering of the band-structure energy. Whereas for the 3×2 AI model the highest occupied surface-state bands appear in a midgap position, this band occurs below the VBM in the 3×2 ADI case.

The findings of semiconducting behavior of Si(113)3×2 surfaces are in agreement with photoemission spectroscopy (PES), angle-resolved photoelectron spectroscopy (ARPES), and STM studies. PES of Ranke and Xing[51] gave the Fermi level in a midgap position of about 0.5 eV above the VBM. This energy region was shown to be free of occupied surface states as demonstrated in Fig. 2(e) for the 3×2 ADI structure. At normal emission and at higher emission angles ARPES (Ref. 21) found two surface bands separated by 0.4 eV below the VBM in a **k**-vector direction parallel to $[1\bar{1}0]$. Along *JK* but also along $J'\Gamma$ (but within the bulk states), we also observe such a pair of surface states in Fig. 2(e). Their splitting is smaller than the measured value. One reason may be the neglect of the quasiparticle corrections. Differential tunneling conductance spectra taken at various sites in the 3×2 unit cell on topographic images for both positive and negative voltages also indicate the existence of surface states for Si(113)3×2.[8] A broad occupied surface-state feature is observed 0.8-eV below the Fermi level, in agreement with PES (Ref. 52) or with a value of 1 eV in Ref. 24. The gap of about 1.2 eV is almost free of surface states, in agreement with the calculations for the 3×2 ADI.

Since within the used DFT-LDA the projected bulk band gap is almost zero at Γ, the interpretation and identification of the surface bands is more complicated for the Ge(113) surface. However, away from the Γ point the situation becomes clear. The slab band structures show a small gap for both the 3×2 AI and the 3×2 ADI models [Figs. 2(d) and 2(e)]. The resulting semiconducting behavior is also confirmed by PES measurements which found the VBM to be 0.22-eV below the Fermi level and this energy region free of surface states.[53]

In order to figure out the true nature of the surface-state bands in the fundamental gap of the projected bulk band structure, the wave functions of the highest occupied (v_1,v_2,v_3) and lowest unoccupied (c_3,c_2,c_1) surface bands are plotted in Figs. 3 and 4. We study 3×1 and 3×2 interstitial reconstructions of the Si(113) surface at the *K* point in the BZ of the 3×2 lattice. At least for Si(113) the states at *K* are well separated from the bulk states and, hence, show a

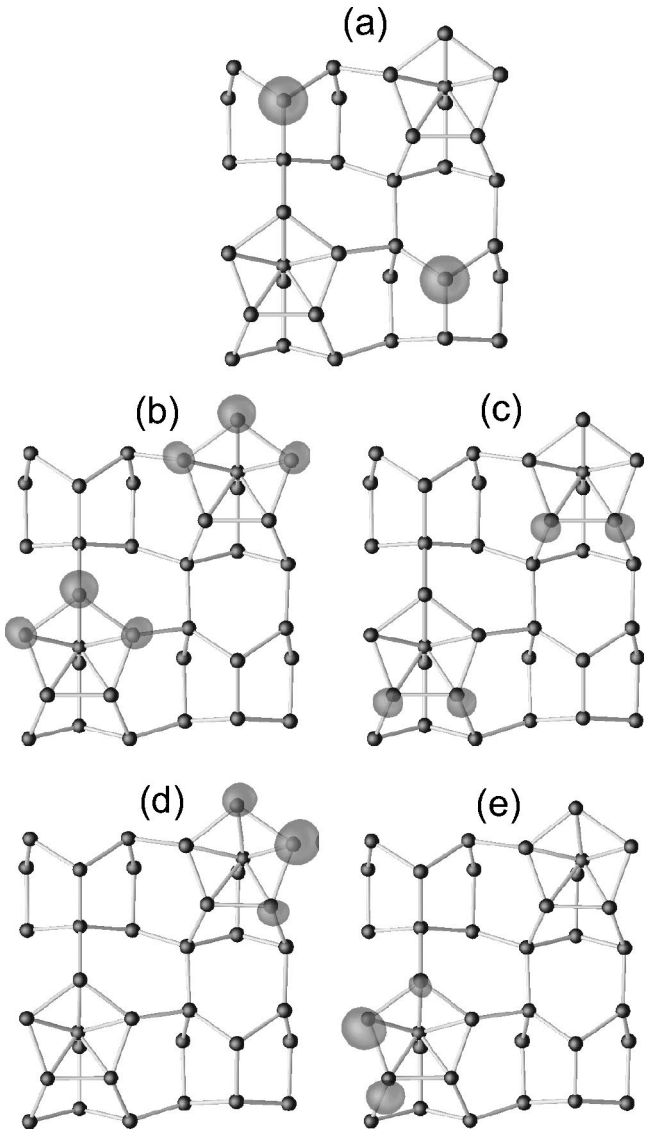

FIG. 3. Wave-function squares of the highest occupied and lowest unoccupied surface bands at K for the Si(113) surface within the 3×1 and 3×2 AI reconstructions. (a) Two fully occupied states $v_{2/3}$, (b) half-occupied v_1/c_1, and (c) the lowest conduction states $c_{2/3}$ of the 3×1 AI model. (d) and (e) Highest occupied (v_1) and lowest unoccupied (c_1) bands of the 3×2 AI surface reconstruction. Corresponding electronic structures with band indication are shown in Figs. 2(c) and 2(d).

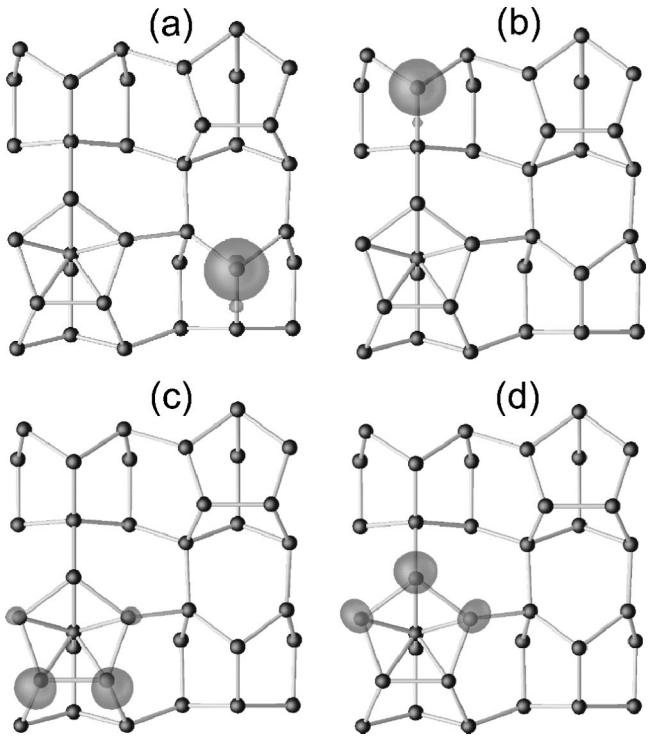

FIG. 4. Wave-function squares of the (v_2,v_1) [(a) and (b)] highest occupied and [(c) and (d)] lowest unoccupied (c_1,c_2) surface bands at K for the Si(113) surface within the 3×2 ADI reconstruction [see Fig. 2(e)].

remarkable localization. In the Ge case there is an energetical overlap of the empty surface bands with the bulk conduction bands at K. Figure 3(a) shows for the 3×1 AI model that the two degenerate surface bands $v_{2/3}$ below the VBM are localized at the adatoms and that each DB of an adatom is completely filled. This filling indicates the main effect of the presence of the interstitials. The DBs at the adatoms are filled and, consequently, adatoms move up (see Table II). The wave functions of the half-filled bands v_1/c_1 in the upper part of the fundamental gap [Fig. 2(c)] are localized at edge atoms and at the subatoms which are originally situated in the third atomic layer. Originally the edge atoms possess half-filled dangling bonds. However, the occurrence of a probability to find electrons at the third-layer atom is somewhat unexpected. That means that this atom is no longer completely fourfold coordinated. Rather, because of the presence of the interstitial, one bond is weakened, allowing the atom in the fourth atomic layer to form a bond with the interstitial atom. Higher states which appear in the gap ($c_{1/2}$) are localized on the dimer atoms [Fig. 2(c)].

The asymmetry in the two pentamers of the 3×2 AI reconstruction governs the gap opening [Fig. 2(d)]. The pentamer atoms, which are closer to the substrate, tend to have more p-like DB states. An electron transfer happens from the electronic states localized at this pentamer into the more s-like states at the pentamer that is somewhat displaced away from the bulk. The difference of buckling in the pentamers also plays a role (Table II). Nevertheless, the atoms with higher altitudes are more filled and contribute to the v_1 [Fig. 3(d)]. The lowest conduction-band states c_1 are localized at the second pentamer [Fig. 3(e)]. The higher states should be observable at the lower parts of the pentamers (not shown).

For the 3×2 ADI model the filled and empty surface states v_1, v_2 and c_1, c_2 are shown in Fig. 4. The occupied states in Figs. 4(a) and 4(b) are again localized at adatoms. The empty states belong to the pentamer [Fig. 4(c) and 4(d)]. Surprisingly, the wave functions around the subsurface interstitial do not contribute to the surface-state bands in the gap. For that reason, they are not visible in STM measurements for not too large voltages.[11,26]

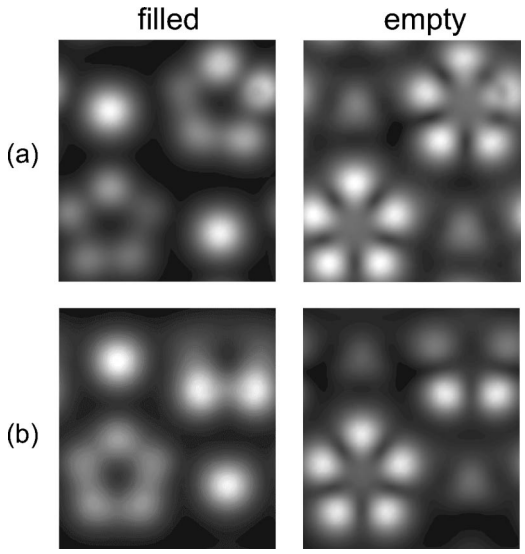

FIG. 5. STM images of filled (left panel) and empty (right panel) states simulated for the (a) 3×2 AI model and (b) 3×2 ADI model of the Si(113) surface.

C. STM images

The different contributions of the empty and filled electronic states localized at the pentamers, tetramers, and the two rebonded adatoms in a certain 3×2 interstitial surface reconstruction will also dominate the STM images. This is demonstrated in Fig. 5 for voltages corresponding to energy intervals of 2-eV below or above the theoretical Fermi level within the fundamental gap in DFT-LDA quality. We present results for Si(113), the 3×2 AI structure, in Fig. 5(a) and for the 3×2 ADI reconstruction in Fig. 5(b). Those for Ge(113) are very similar. The main differences are due to the strength of the buckling within the 3×2 AI reconstruction.

The resulting STM images are in accordance with the discussion of the orbital character of the gap states in Figs. 3 and 4. Figure 5(a) for the 3×2 AI model clearly shows that the filled-state images are dominated by the wave functions localized at the adatoms. The two pentamers are less visible. However, the right part of the upper pentamer shows brighter spots. They are related to the pronounced asymmetry of the two pentamers. The empty-state images show opposite behavior. The pentamers are clearly visible, whereas only weak contributions are associated with the adatoms. The asymmetry in the upper pentamer is indicated by somewhat smeared-out spots. The interstitial atoms are not visible. In principle, such nonsymmetric pentamers are observed experimentally for seeming 3×1 areas of the Ge(113) surface.[28] Although the asymmetry can be seen there, it is difficult to distinguish whether the 3×1 or 3×2 AI reconstruction appears on the surface, at least in empty-state images. Consequently it is also difficult to distinguish between 3×1 or 3×2 translational symmetries using a local method such as STM.

The observation of pentamerlike structures in empty-state images[8,12,27] should be taken as an indication for an interstitial. This is clearly shown in Fig. 5(b) for the 3×2 ADI model by the differences between spot arrangements related to pentamers or tetramers. The dimer atoms in the upper-right feature appear in both empty-state and filled-state images, whereas the pentamer is more (empty state) or less (filled state) visible. More in detail, the filled-state image is dominated by electronic states localized at the adatoms, as in the case with two interstitials, i.e., the 3×2 AI (or 3×1 AI) reconstruction. For Si(113)3×2,[12] as well as Ge(113)3×2,[28] such filled-state images have indeed been observed. The adatoms obtain electrons from the pentamers to fill their partially occupied states. In the empty-state image [Fig. 5(b), right] the adatoms are not seen. The pentamer can be well identified, while the tetramer is only partially visible due to empty π^* dimer states. Images of this type have been observed for Si(113)3×2 surfaces and voltages of 3 V.[12] The observation of the dimer in the tetramer in both images is related to the bonding and antibonding π states of these atoms. This is not surprising since the corresponding bands do not appear in the fundamental gap and are resonant with the projected bulk band structure. Therefore, for smaller voltages, the dimers (and the entire tetramers) should be less visible in both filled-state and empty-state images. Finally we must mention that the images have been calculated assuming a constant-height mode and not a constant-current mode, and that the energy interval of 2 eV used in the calculations of the images means a larger value for the experimental voltage, since the quasiparticle gap opening is not taken into account.

IV. CONCLUSIONS

In summary, *ab initio* calculations have been performed to study different reconstructions of C, Si, and Ge(113) surfaces with 3×1 and 3×2 translational symmetries. Reconstruction models including dimers, rebonded adatoms, and subsurface interstitials have been studied. The absolute surface energies, the minimum-energy geometries, the band structures, and STM images have been computed.

For diamond the most stable reconstruction is described by the 3×1 AD model without buckling or puckering. This result agrees with the tendency found for C(001)2×1 and C(111)2×1 surfaces that subsurface strains cost too much energy and that additional atoms, e.g., adatoms in the (111) case, are energetically unfavorable. However, as for the C(111)2×1 surface, a surface band structure of a two-dimensional metal is calculated, at least within the used DFT-LDA. This result needs further discussion. In any case, the absolute surface energy of a C(113)3×1 surface is so low that corresponding facets should occur on the equilibrium crystal shape, i.e., the (113) surfaces are also stable for diamond.

The Si and Ge(113) surfaces are confirmed to be stabilized by subsurface self-interstitials. For germanium two considered interstitial-induced reconstructions, 3×1 AI and 3×2 ADI, can be hardly distinguished from an energetical point of view. The 3×2 AI reconstruction gives rise to a global minimum on the total-energy surface. Nevertheless, the small energy differences indicate that the interstitial migration and coexistence of different surface phases should be likely. In the Si(113) case, due to a repulsive interaction of the interstitial atoms on short distances, the 3×2 ADI struc-

ture is found to be most favorable. However, the energy differences to the other interstitial reconstructions remain also small. For both Ge and Si the comparison with the absolute surface energies of the low-index surfaces shows that (113) surfaces should give stable facets. They should clearly appear on the equilibrium crystal shape and not decay into smaller flat areas with (111) and (001) orientations. Within the stable reconstructions of the Si and Ge(113) surfaces only the 3×2 AI and 3×2 ADI structures give rise to insulating (semiconducting) band structures. The calculated electronic structures, in particular, that of the 3×2 ADI for Si(113), seem to agree with the available experimental data from PES, ARPES, and STM. Important facts concern the occurrence of occupied surface states below the VBM and strong asymmetry in the filled- and empty-state images. The energetics, the gap opening, and the similarities of the STM images suggest the interpretation of the experimental data available for ordered (113) Si and Ge surfaces in terms of the 3×2 translational symmetry.

ACKNOWLEDGMENT

We acknowledge financial support from the Deutsche Forschungsgemeinschaft (Project No. Be1346/12-1) and the European Community in the framework of the Research and Training Network NANOPHASE (Contract No. HPRN-CT-2000-00167).

[1] D.J. Eaglesham, A.E. White, L.C. Feldman, N. Moriya, and D.C. Jacobson, Phys. Rev. Lett. **70**, 1643 (1993).
[2] H. Omi and T. Ogino, Phys. Rev. B **59**, 7521 (1999).
[3] B. Voigtländer and A. Zinner, Appl. Phys. Lett. **63**, 3055 (1993).
[4] G. Medeiros-Ribeiro, A.M. Bratkovski, T.I. Kamins, D.A.A. Ohlberg, and R.S. Williams, Science (Washington, DC, U.S.) **279**, 353 (1998).
[5] B. Schröter, K. Komlev, U. Kaiser, G. Hess, G. Kipshidze, and W. Richter, Mater. Sci. Forum **353-356**, 247 (2001); K. Komlev, B. Schröter, and W. Richter (unpublished).
[6] G. Janssen, J.J. Schermer, W.J.P. van Enckevort, and L.J. Giling, J. Cryst. Growth **125**, 42 (1992).
[7] W. Ranke, Phys. Rev. B **41**, 5243 (1990).
[8] J. Knall, J.B. Pethica, J.D. Todd, and J.H. Wilson, Phys. Rev. Lett. **66**, 1733 (1991).
[9] U. Myler, P. Althainz, and K. Jacobi, Surf. Sci. **251/252**, 607 (1991).
[10] J. Schreiner, K. Jacobi, and W. Selke, Phys. Rev. B **49**, 2706 (1994).
[11] J. Dabrowski, H.-J. Müssig, and G. Wolf, Surf. Sci. **331-333**, 1022 (1995).
[12] H. Sakama, D. Kunimatsu, M. Kageshima, and A. Kawazu, Phys. Rev. B **53**, 6927 (1996).
[13] H. Hibino and T. Ogino, Phys. Rev. B **56**, 4092 (1997).
[14] Z. Gai, R.G. Zhao, and W.S. Yang, Phys. Rev. B **56**, 12 303 (1997).
[15] T. Suzuki, H. Minoda, Y. Tanishiro, and K. Yagi, Surf. Rev. Lett. **5**, 249 (1998).
[16] H. Vogler, A. Iglesias, W. Moritz, and H. Over, Phys. Rev. B **57**, 2315 (1998).
[17] H. Ikeda, Y. Oshima, H. Hirayama, and K. Takayanagi, Surf. Sci. **433-435**, 632 (1999).
[18] A. Iglesias, M. Gierer, D. Wolf, and W. Moritz, Surf. Sci. **442**, 357 (1999).
[19] C.C. Hwang, H.S. Kim, Y.K. Kim, J.S. Kim, C.Y. Park, K.J. Kim, T.-H. Kang, and B. Kim, Phys. Rev. B **59**, 14 864 (1999).
[20] C.Y. Chang, Y.C. Chou, and C.M. Wei, Phys. Rev. B **59**, R10 453 (1999).
[21] K.S. An, C.C. Hwang, H.S. Kim, C.-Y. Park, I. Matsuda, H.W. Yeom, S. Suga, and A. Kakizaki, Surf. Sci. **478**, 123 (2001).
[22] M. Takeguchi, M. Tanaka, H. Yasuda, and K. Furuya, Surf. Sci. **482-485**, 1385 (2001).
[23] C.C. Hwang, H.S. Kim, Y.K. Kim, K.W. Ihm, C.Y. Park, K.S. An, K.J. Kim, T.-H. Kang, and B. Kim, Phys. Rev. B **64**, 045305 (2001).
[24] C.C. Hwang, K.-J. Kim, T.-H. Kang, B. Kim, Y. Chung, and C.Y. Park, Surf. Sci. **514**, 319 (2002).
[25] J. Wang, A.P. Horsfield, D.G. Pettifor, and M.C. Payne, Phys. Rev. B **54**, 13 744 (1996).
[26] J. Dabrowski, H.-J. Müssig, and G. Wolff, Phys. Rev. Lett. **73**, 1660 (1994).
[27] J. Dabrowski, H.-J. Müssig, and G. Wolff, J. Vac. Sci. Technol. B **13**, 1597 (1995).
[28] A. Laracuente, S.C. Erwin, and L.J. Whitman, Phys. Rev. Lett. **81**, 5177 (1998).
[29] D.M. Bird, L.J. Clarke, R.D. King-Smith, M.C. Payne, I. Stich, and A.P. Sutton, Phys. Rev. Lett. **69**, 3785 (1992).
[30] Y.P. Feng, T.H. Wee, C.K. Ong, and H.C. Poon, Phys. Rev. B **54**, 4766 (1996).
[31] K.A. Feng, X.M. Hu, Z. Lin, and Y.R. Xing, Appl. Surf. Sci. **120**, 94 (1997).
[32] C.B. Duke, Chem. Rev. (Washington, DC, U.S.) **96**, 1237 (1996).
[33] M.D. Pashley, Phys. Rev. B **40**, 10 481 (1989).
[34] P. Hohenberg and W. Kohn, Phys. Rev. **136**, B864 (1964).
[35] W. Kohn and L.J. Sham, Phys. Rev. **140**, A1133 (1965).
[36] J.P. Perdew and A. Zunger, Phys. Rev. B **23**, 5048 (1981).
[37] J.P. Perdew, J.A. Chevary, S.H. Vosko, K.A. Jackson, M.R. Pederson, D.J. Singh, and C. Fiolhais, Phys. Rev. B **46**, 6671 (1992).
[38] D. Vanderbilt, Phys. Rev. B **41**, 7892 (1990).
[39] S.G. Louie, S. Froyen, and M.L. Cohen, Phys. Rev. B **26**, 1738 (1982).
[40] J. Furthmüller, P. Käckell, F. Bechstedt, and G. Kresse, Phys. Rev. B **61**, 4576 (2000).
[41] G. Kresse and J. Furthmüller, Comput. Mater. Sci. **6**, 15 (1996); Phys. Rev. B **54**, 11 169 (1996).
[42] A.A. Stekolnikov, J. Furthmüller, and F. Bechstedt, Phys. Rev. B **65**, 115318 (2002).
[43] M.S. Hybertsen and S.G. Louie, Phys. Rev. B **34**, 5390 (1986).
[44] F. Bechstedt, Adv. Solid State Phys. **32**, 161 (1992).

[45] J. Tersoff and D.R. Hamann, Phys. Rev. B **31**, 805 (1985).
[46] P. Krüger and J. Pollmann, Phys. Rev. Lett. **74**, 1155 (1995).
[47] A. Scholze, W.G. Schmidt, and F. Bechstedt, Phys. Rev. B **53**, 13 725 (1996).
[48] F. Bechstedt, W.G. Schmidt, and A. Scholze, Europhys. Lett. **35**, 585 (1996).
[49] G. Wulff, Z. Kristallogr. Mineral. **34**, 44 (1901).
[50] C. Herring, Phys. Rev. **82**, 87 (1951).
[51] W. Ranke and Y.R. Xing, Phys. Rev. B **31**, 2246 (1985).
[52] U. Myler and K. Jacobi, Surf. Sci. **220**, 353 (1989).
[53] S.M. Sholz, J. Schreiner, and K. Jacobi, Surf. Sci. **331**, 402 (1995).